

On the Analysis and Kinematic Design of a Novel 2-DOF Translational Parallel Robot

Jinsong Wang, Xin-Jun Liu and Chao Wu

1. Introduction

The conceptual design of parallel robots can be dated back to the time when Gough established the basic principles of a device with a closed-loop kinematic structure (Gough 1956), that can generate specified position and orientation of a moving platform so as to test tire wear and tear. Based on this principle, Stewart designed a platform for use as an aircraft simulator in 1965 (Stewart 1965). In 1978, Hunt (1978) made a systematic study of robots with parallel kinematics, in which the planar 3-RPS (R-revolute joint, P-prismatic joint, and S-spherical joint) parallel robot is a typical one. Since then, parallel robots have been studied extensively by numerous researchers.

The most studied parallel robots are with 6 DOFs. These parallel robots possess the advantages of high stiffness, low inertia, and large payload capacity. However, they suffer the problems of relatively small useful workspace and design difficulties (Merlet 2000). Furthermore, their direct kinematics possess a very difficult problem; however the same problem of parallel robots with 2 and 3 DOFs can be described in a closed form (Liu 2001). As is well known, there are three kinds of singularities in parallel robots (Gosselin and Angeles 1990). Moreover, not all singularities of a 6-DOF parallel robot can be found easily. But for a parallel robot with 2 and 3 DOFs, the singularities can always be identified readily. For such reasons, parallel robots with less than 6 DOFs, especially 2 and 3 DOFs, have increasingly attracted more and more researchers' attention with respect to industrial applications (Tsai & Stamper 1996; Ceccarelli 1997; Tonshoff et al 1999; Siciliano 1999; Liu et al. 2001; Liu et al. 2005; Liu & Kim 2003). In these designs, parallel robots with three translational DOFs have been playing important roles in the industrial applications (Tsai & Stamper 1996; Clavel 1988; Hervé 1992; Kim & Tsai 2002; Zhao & Huang 2000; Carricato & Parenti-Castelli 2001; Kong & Gosselin 2002; Liu et al. 2003), especially, the DELTA robot (Clavel 1988), which is evident from the fact that the design of the DELTA robot is covered by a family of 36 patents (Bonev 2001). Tsai's robot (Tsai & Stamper 1996), in which each of the three legs consists of a parallelogram, is the first design to solve the problem of UU chain. A 3-

translational-DOF parallel robot, Star, was designed by Hervé based on group theory (Hervé 1992). Such parallel robots have wide applications in the industrial world, e.g., pick-and-place application, parallel kinematic machines, and medical devices.

The most famous planar 2-DOF parallel robots (Asada & Kanade 1983; McCloy 1990; Gao et al. 1998) are the well-known five-bar mechanism with prismatic actuators or revolute actuators. In the case of the robot with revolute actuators, the mechanism consists of five revolute pairs and the two joints fixed to the base are actuated. In the case of the robot with prismatic actuators, the mechanism consists of three revolute pairs and two prismatic joints, in which the prismatic joints are usually actuated. The output of the robot is the translational motion of a point on the end-effector, i.e., the orientation of the end-effector is also changed correspondingly. Accordingly, some versions of the 2-DOF translational parallel robot (TPR) have been disclosed. One of them has been applied in precise pick & place operations at high speed in IWF at Technical University of Braunschweig. In 2001, another 2-DOF TPR has been proposed for the conceptual design of a 5-axis machine tool (Liu 2001). The structure, kinematics and dynamics of the TPR were discussed in details (Liu et al., 2002; Liu et al., 2005). Recently, a 2-DOF TPR with revolute actuators was introduced (see Table 1 in (Liu & Wang, 2003); Huang et al., 2004). The TPR presented in (Liu 2001; Liu et al., 2005) has been used in the design of a planer machine tool with a gantry structure instead of a traditional one with serial chains to improve its stiffness and inertia characteristics. However, all of these TPRs consist of at least of one parallelogram. Here, a novel 2-DOF TPR with only revolute and prismatic joints will be proposed. The robot can position an objective with constant orientation with high speed.

As it is one of the most important and challenging issues in the parallel robot, optimal kinematic design has drawn more and more researchers' attention (Gosselin & Angeles, 1989; Chablat & Wenger, 2003; Stock & Miller, 2004; Ottaviano & Ceccarelli, 2002; Cervantes-Sánchez et al., 2001). The objective of optimal kinematic design is determining the dimension or link length of a robot with respect to desired performance(s). Due to the parameter infinity and the instability of performance in a whole workspace, optimal kinematic design is one of the most challenging problems in the field of parallel robot. The commonly used methods are first to develop an objective function and then to reach the result using the numerical method with an algorithm. These methodologies have the disadvantages in common, i.e., the objective function is difficult to be established; the numerical procedure may lead to a solution that is quite far away from the optimal solution; the process is iterative and time consuming; and, most fatally, only one optimal solution can be provided. To overcome the disadvantages, in this chapter, a new optimal design methodology will be proposed for the parallel robot. Using a normalization method, the dimensional characteristic parameters of the robot will be normalized. The nor-

malization can guarantee that a dimensional robot and its corresponding normalized robot are similar not only in size but also in performance. The dimensional robot is defined as *similarity robot* (SR), and the normalized robot is referred to as *basic similarity robot* (BSR). A design space which embodies all kinds of BSRs will be established. The space can be used not only in analysis but also in the optimal design of the parallel robot. Within the design space, the performance atlas that illustrates the relationship between a performance index and the BSRs can be plotted. The optimal kinematic design can be implemented with respect to the performance atlases. Design examples will be finally given in the chapter. Compared with the traditional design methods, the proposed optimal design methodology has some advantages as follows: (a) one performance index corresponds to one atlas; (b) for such a reason in (a), the fact that some performance indices are antagonistic is no longer a problem in the design; (c) the optimal design process can consider multi-objective functions or multi-indices, and also guarantees the optimal result; and finally, (d) the design method provides a set of possible solutions, and ideally, all the design solutions.

2. Description of the 2-DOF TPR and its Topological Architectures

2.1 Architecture description

The novel 2-DOF translational parallel robot proposed here is shown in Fig. 1(a). A schematic of the robot is shown in Fig. 1(b). The end-effector of the robot is connected to the base by two kinematic legs 1 and 2. Leg 1 consists of three revolute joints and leg 2 two revolute joints and one cylinder joint, or three revolute joints and one prismatic joint. In each leg, the revolute joints are parallel to each other. The axes of the revolute joints in leg 1 are normal to those of the joints in leg 2. The two joints attached to the end-effector are put in the adjacent sides of a square. The kinematic chain of the robot is denoted as RRR-RRC (C-cylinder joint) or RRR-RRRP.

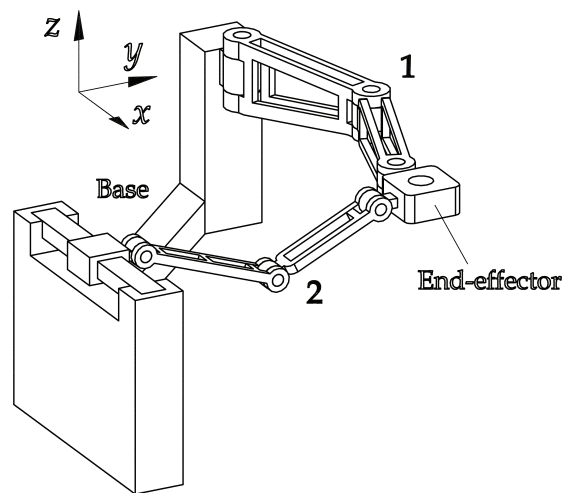
2.2 Capability

Here, a Plücker coordinate like $\$j = (\bar{x}, \bar{y}, \bar{z}; \hat{x}, \hat{y}, \hat{z})$ is used to describe the capability of an object j . In $\$j$, $Tr_j = (\bar{x}, \bar{y}, \bar{z})$ and $Ro_j = (\hat{x}, \hat{y}, \hat{z})$ express the translation and rotation of the object, respectively. If an element in $\$$ is equal to 0, there is no such a translation or rotation. If it is equal to 1, there is the capability. For example, $\bar{x} = 0$ means that the object has no the translation along the x -axis; $\hat{y} = 1$ indicates that the object can rotate about the y -axis.

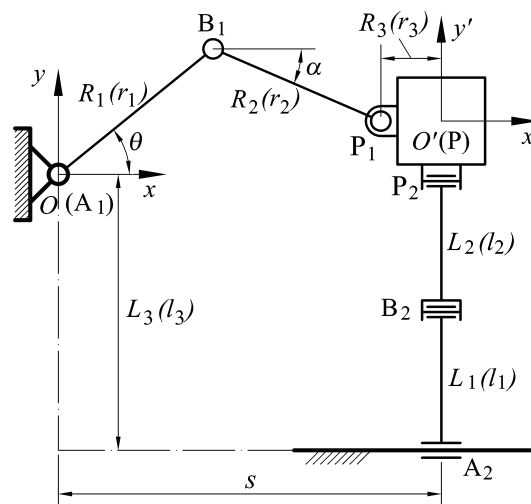
Observing only the leg 1, the Plücker coordinate of the end-effector in the leg can be written as $\$1=(1, 1, 0; 0, 0, 1)$. Letting the leg 1 alone, the Plücker coordinate of the end-effector with the leg 2 can be expressed as $\$2=(1, 1, 1; 1, 0, 0)$. Then, the intersection of the two Plücker coordinates $\$1$ and $\$2$ is $\$$, i.e.,

$$\$=\$1 \cap \$2=(1, 1, 0; 0, 0, 1) \cap (1, 1, 1; 1, 0, 0)=(1, 1, 0; 0, 0, 0) \quad (1)$$

which describes the capability of the robot, i.e., the translations of the end-effector along the x and y axes. That means the end-effector has two purely translational degrees of freedom with respect to the base.



(a)



(b)

Figure 1. The 2-DOF translational parallel robot: (a) the CAD model; (b) the schematic

2.3 Topological architectures

Observing the robot shown in Fig. 1, it is not difficult to reach such a conclusion that if the axes of the joints in the leg 1 are normal to those of the joints in the leg 2 the robot will have two translational DOFs. Based on this idea, some topological architectures are shown in Fig. 2. It is noteworthy that the leg 2 shown in Fig. 1 and Fig. 2 can be also the kinematic chain RRR(Pa) shown in Fig. 3, where Pa means planar parallelogram.

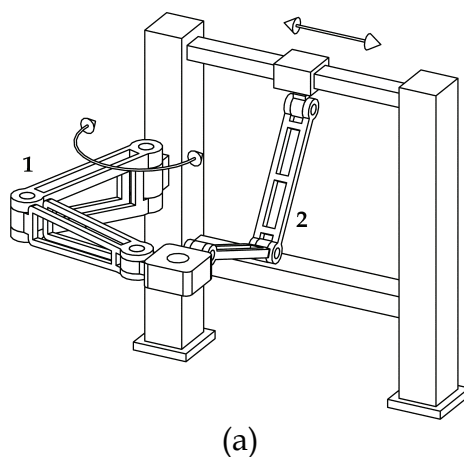
3. Kinematics Analysis

Although the robot has some topologies, this chapter considers only the architecture shown in Fig. 1. In this section, the inverse and forward kinematics of the robot will be given.

3.1 Inverse kinematics

As illustrated in Fig. 1(b), a reference frame $\mathfrak{R} : O - xy$ is fixed to the base at the joint point A_1 and a moving reference frame $\mathfrak{R}' : O' - x'y'$ is attached to the end-effector, where O' is the reference point on the end-effector. Vectors $\mathbf{p}_{i\mathfrak{R}}$ ($i = 1, 2$) will be defined as the position vectors of points P_i in frames \mathfrak{R} , and vectors $\mathbf{b}_{i\mathfrak{R}}$ ($i = 1, 2$) as the position vectors of points B_i in frame \mathfrak{R} . The geometric parameters of the robot are $A_1B_1 = R_1(r_1)$, $B_1P_1 = R_2(r_2)$, $PP_1 = R_3(r_3)$, $A_2B_2 = L_1(l_1)$, $B_2P_2 = L_2(l_2)$, and the distance between the point A_1 and the guideway is $L_3(l_3)$, where R_n and L_n ($n=1,2,3$) are dimensional parameters, and r_n and l_n non-dimensional parameters. The position of point O' in the fixed frame \mathfrak{R} is denoted as vector

$$\mathbf{c}_{\mathfrak{R}} = (x, y)^T \tag{2}$$



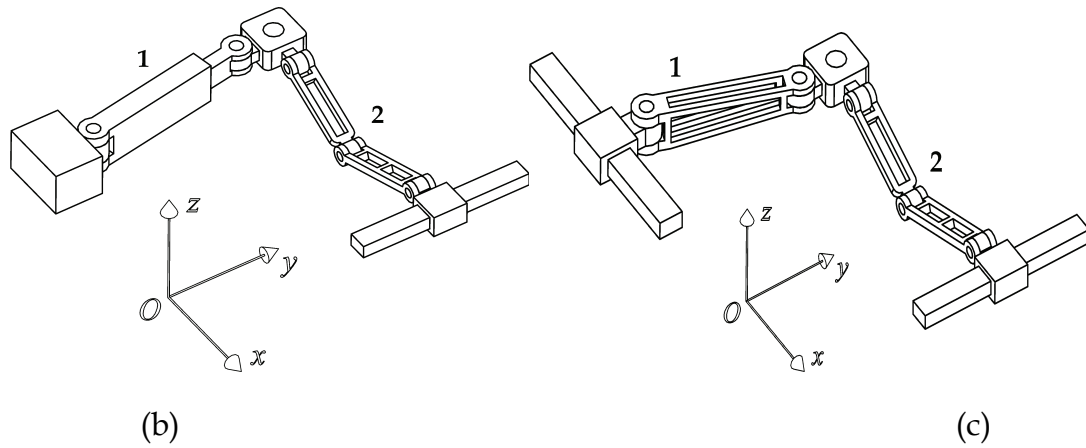


Figure 2. Some topological architectures: (a) RRR-RRRP chain (arrangement is different from that shown in Fig. 1); (b) RPR-RRRP chain; (c) PRR-RRRP chain.

The vectors of $\mathbf{b}_{1\mathfrak{R}}$ in the fixed frame \mathfrak{R} can be written as

$$\mathbf{b}_{1\mathfrak{R}} = (R_1 \cos \theta \quad R_1 \sin \theta)^T \quad (3)$$

where θ is the actuated input for the leg 1. Vector $\mathbf{p}_{1\mathfrak{R}}$ in the fixed frame \mathfrak{R} can be written as

$$\mathbf{p}_{1\mathfrak{R}} = (-R_3 \quad 0)^T + \mathbf{c}_{\mathfrak{R}} = (x - R_3 \quad y)^T \quad (4)$$

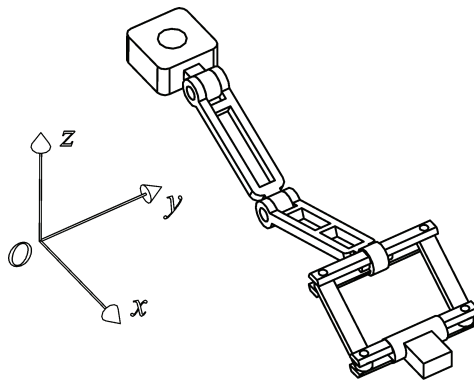


Figure 3. One topological architecture of the leg 2

The inverse kinematics problem of the leg 1 can be solved by writing following constraint equation

$$\|\mathbf{p}_{1\mathfrak{R}} - \mathbf{b}_{1\mathfrak{R}}\| = R_2 \quad (5)$$

that is

$$(x - R_3 - R_1 \cos \theta)^2 + (y - R_1 \sin \theta)^2 = R_2^2 \quad (6)$$

Then, there is

$$\theta = 2 \tan^{-1}(m) \quad (7)$$

where

$$m = \frac{-b + \sigma \sqrt{b^2 - 4ac}}{2a} \quad (8)$$

$$\sigma = 1 \text{ or } -1$$

$$a = (x - R_3)^2 + y^2 + R_1^2 - R_2^2 + 2(x - R_3)R_1$$

$$b = -4yR_1$$

$$c = (x - R_3)^2 + y^2 + R_1^2 - R_2^2 - 2(x - R_3)R_1$$

For the leg 2, it is obvious that

$$s = x \quad (9)$$

in which s is the input of the leg 2. From Eqs. (8) and (9), we can see that there are two solutions for the inverse kinematics of the robot. Hence, for a given robot and for prescribed values of the position of the end-effector, the required actuated inputs can be directly computed from Eqs. (7) and (9). To obtain the configuration as shown in Fig.1, parameter σ in Eq. (8) should be 1. This configuration is called the “+” working mode. When $\sigma = -1$, the corresponding configuration is referred to as the “-” working mode.

3.2 Forward kinematics

The forward kinematic problem is to obtain the output with respect to a set of given inputs. From Eqs. (6) and (9), one obtains

$$y = e + \sigma \sqrt{f} \quad (11)$$

and

$$x = s \quad (12)$$

where, $e = R_1 \sin \theta$ and $f = R_2^2 - (s - R_3 - R_1 \cos \theta)^2$. Therefore, there are also two forward kinematic solutions for the robot. The parameter $\sigma = -1$ corre-

sponds to the configuration shown in Fig. 1, which is denoted as the *down-configuration*. When $\sigma = 1$, the configuration is referred to as the *up-configuration*. These two kinds of configurations correspond to two kinds of assembly modes of the robot.

Figure 4 illustrates two kinds of working modes of the robot. The two kinds of assembly modes are shown in Fig. 5. In this chapter, the robot with both the “+” working mode and *down-configuration* will be considered only.

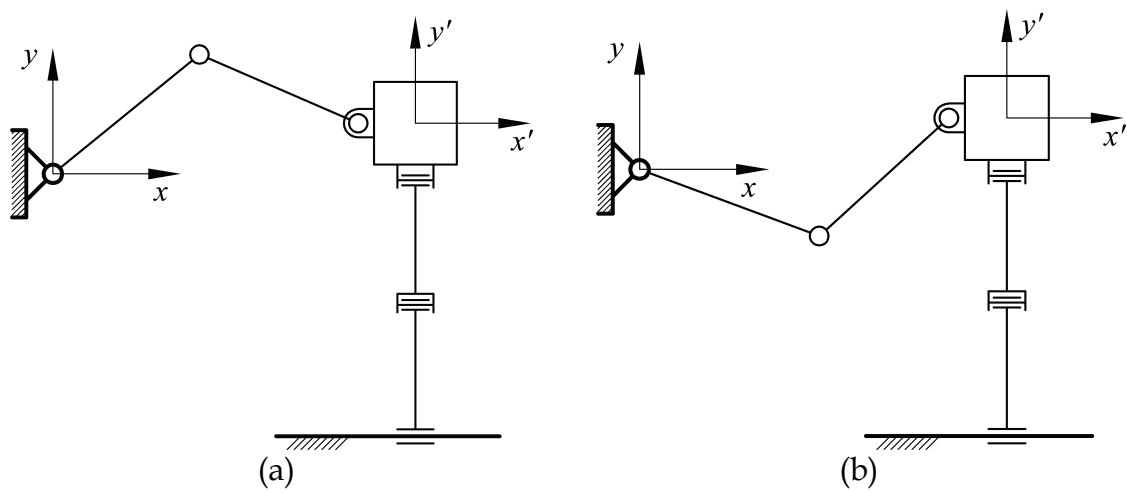


Figure 4. Two kinds of working modes: (a) “+” working mode; (b) “-” working mode

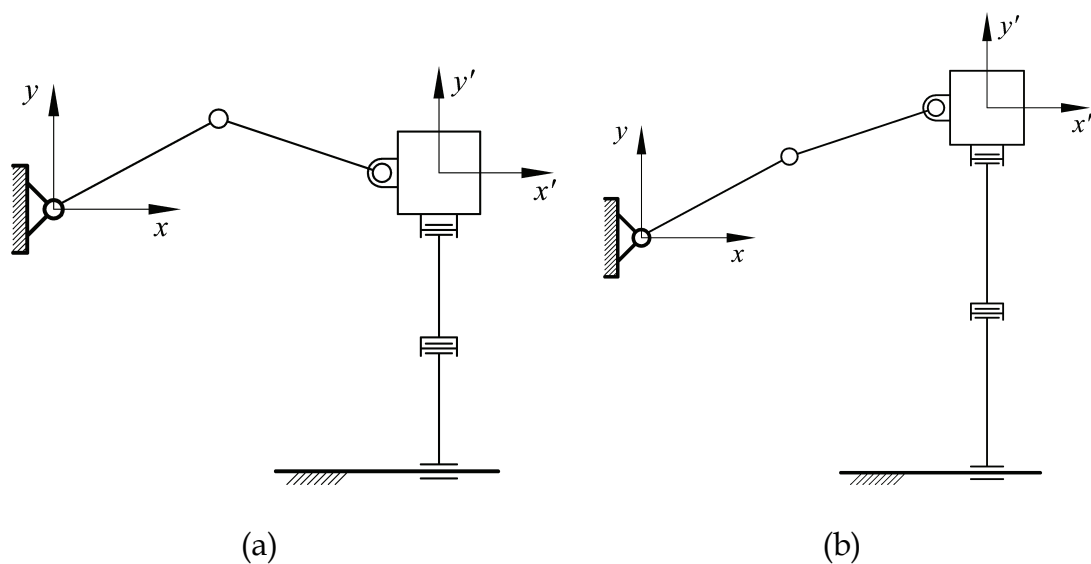


Figure 5. Two kinds of assembly modes: (a) *down-configuration*; (b) *up-configuration*

4. Singularity Analysis

4.1 Jacobian matrix

Equations (6) and (9) can be differentiated with respect to time to obtain the velocity equations. This leads to

$$\dot{s} = \dot{x} \quad (13)$$

$$R_1[y \cos \theta - (x - R_3) \sin \theta] \dot{\theta} = (x - R_3 - R_1 \cos \theta) \dot{x} + (y - R_1 \sin \theta) \dot{y} \quad (14)$$

which can be written in an equation of the form

$$A \dot{q} = B \dot{p} \quad (15)$$

where $\dot{q} = (\dot{s} \ \dot{\theta})^T$ and $\dot{p} = (\dot{x} \ \dot{y})^T$ are the joint and Cartesian space velocity vectors, respectively, and A and B are, respectively, the 2×2 matrices and can be expressed as

$$A = \begin{bmatrix} 1 & 0 \\ 0 & R_1 y \cos \theta - R_1 (x - R_3) \sin \theta \end{bmatrix}, \text{ and } B = \begin{bmatrix} 1 & 0 \\ x - R_3 - R_1 \cos \theta & y - R_1 \sin \theta \end{bmatrix} \quad (16)$$

If matrix A is nonsingular, the Jacobian matrix of the robot can be obtained as

$$J = A^{-1}B = \begin{bmatrix} 1 & 0 \\ \frac{x - R_3 - R_1 \cos \theta}{R_1 y \cos \theta - R_1 (x - R_3) \sin \theta} & \frac{y - R_1 \sin \theta}{R_1 y \cos \theta - R_1 (x - R_3) \sin \theta} \end{bmatrix} \quad (17)$$

from which one can see that there is no any parameter of L_n ($n=1,2,3$) in this matrix.

4.2 Singularity

In the parallel robot, singularities occur whenever A , B or both, become singular. As a singularity leads to an instantaneous change of the robot's DOF, the analysis of parallel robots has drawn considerable attention. For the parallel robot studied here, since there is no any parameter of the leg 2 involved in the Jacobian matrix (see Eqs. (16) and (17)), the singularity is actually only that of the leg 1.

The stationary singularity occurs when A becomes singular but B remains invertible. $|A|=0$ leads to $R_1 y \cos \theta - R_1 (x - R_3) \sin \theta = 0$, i.e. $\tan \theta = y / (x - R_3)$.

Physically, this corresponds to the configuration when leg 1 $A_1B_1P_1$ is completely extended or folded. This singularity is also referred to as the serial singularity. For example, for the robot with the parameters $R_1 = 1.2\text{mm}$ and $R_2 = 0.8\text{mm}$, two configurations of this kind of singularity are shown in Fig. 6. The loci of point P for this kind of singularity can be expressed as

$$C_{fir_o}: (x - R_3)^2 + y^2 = (R_1 + R_2)^2 \quad (18)$$

and

$$C_{fir_i}: (x - R_3)^2 + y^2 = (R_1 - R_2)^2 \quad (19)$$

For the above example, if $R_3 = 0.5\text{mm}$ the loci of point P are shown in Fig. 7.

Note that, $R_1 = 0$ leads to $\det(\mathbf{A}) = 0$ as well. Therefore, $R_1 = 0$ also results in this kind of singularity.

The uncertainty singularity, occurring only in closed kinematics chains, arises when \mathbf{B} becomes singular but \mathbf{A} remains invertible. $|\mathbf{B}| = 0$ results in $y = R_1 \sin \theta$. Physically, this corresponds to the configuration when link B_1P_1 is parallel to the x -axis. Two such configurations are shown in Fig. 8. In such a singularity, the loci of point P can be written as

$$C_{sec_r}: (x - R_3 - R_2)^2 + y^2 = R_1^2 \quad (20)$$

and

$$C_{sec_l}: (x - R_3 + R_2)^2 + y^2 = R_1^2 \quad (21)$$

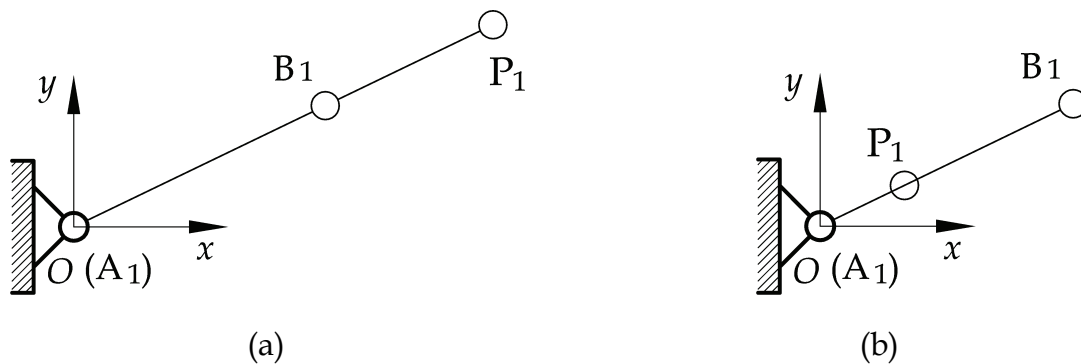


Figure 6. Two kinds configurations of the stationary singularity: (a) $A_1B_1P_1$ is completely extended; (b) $A_1B_1P_1$ is completely folded

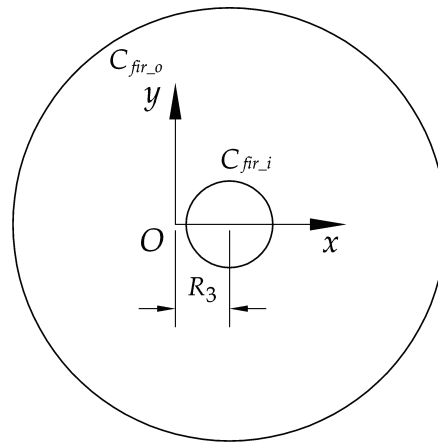


Figure 7. Singular loci of point P when the robot is in the stationary singularity

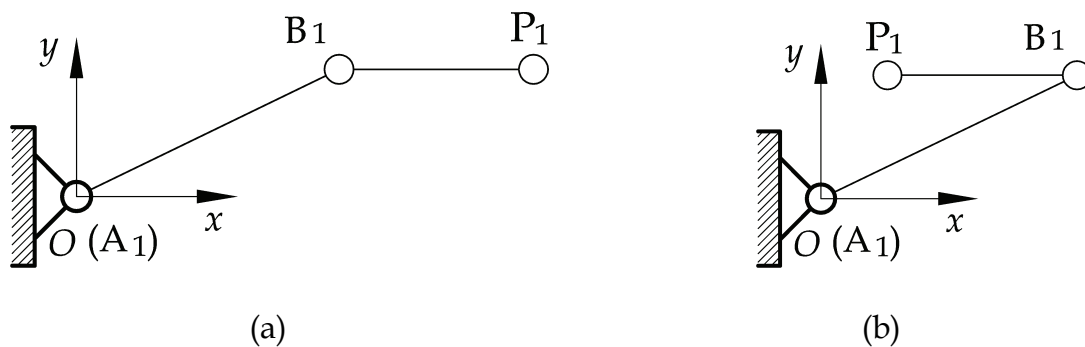


Figure 8. Two kinds configurations of the uncertainty singularity: (a) point P_1 is in the right of point B_1 ; (b) point P_1 is in the left of point B_1

It is noteworthy that the singular loci of a robot when R_1 is greater than R_2 is different from those when R_2 is greater than R_1 . The two cases are shown in Fig. 9. From Figs. 7 and 9, we can see that the uncertainty singular loci are always inside the region bounded by the stationary singular loci; and there are usually tangent points between the two kinds of loci.

The analysis on the kinematics of the robot shows that there are two solutions for both the inverse and forward kinematics. Any one of the singularities will result in the change of solution number of the kinematics. For example, the stationary singularity leads to the loss of solution number of the inverse kinematics. While in the uncertainty singular configuration, the solution number of the forward kinematics can be less or more than two. Then the stationary singularity can be called the inverse kinematic singularity, and the uncertainty singularity the forward kinematic singularity.

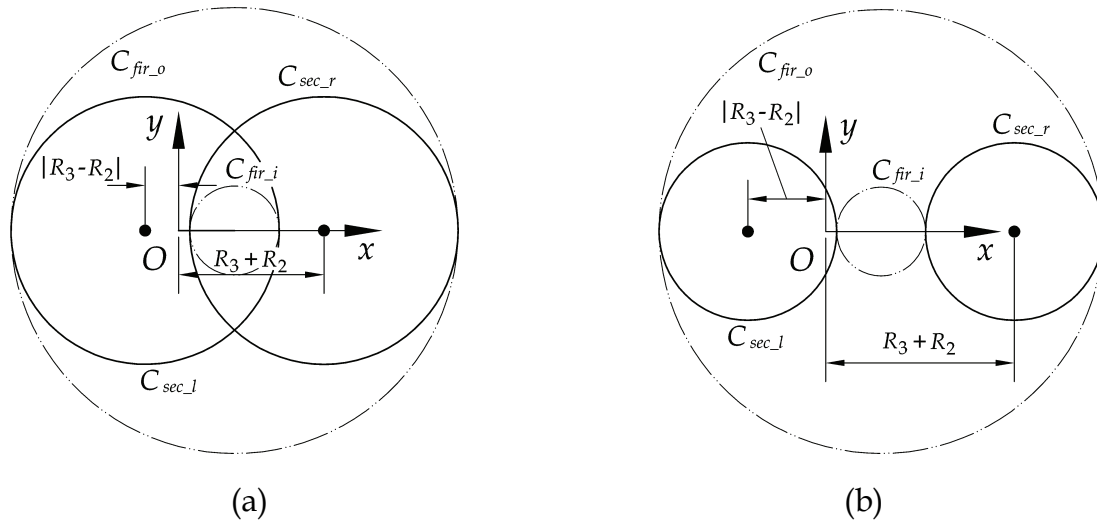


Figure 9. Singular loci of point P when the robot is in the stationary singularity: (a) $R_1 \geq R_2$; (b) $R_1 < R_2$

5. Workspace Analysis

One of the most important issues in the design process of a robot is its workspace. For parallel robots, this issue may be more critical since parallel robots will sometimes have rather a limited workspace.

5.1 Theoretical workspace

Theoretical workspace of the studied robot is defined as the region that the output point can reach if θ changes from 0 to 2π and s between $-\infty$ and ∞ without the consideration of interference between links and the singularity.

From Eq. (6), one can see that if θ is specified, the workspace of the leg 1 is a circle centered at the point $(R_1 \cos \theta + R_3, R_1 \sin \theta)$ with a radius of R_2 . The circle is denoted as C_{11} . If θ_i changes from 0 to 2π , the center point is located at a circle centered at point $(R_3, 0)$ with a radius of R_1 . The circle is denoted as C_{12} . Then, the workspace of the leg is the enveloping region of the circle C_{11} when its center rolls at the circle C_{12} . Actually, the enveloping region is an annulus bounded by two circles C_{fir_o} and C_{fir_i} given in Eqs. (18) and (19), respectively. Especially, when $R_1 = R_2$ the workspace is the region bounded by the circle C_{fir_o} .

Thinking about the architecture of the studied parallel robot, we can see that the workspace of leg 1 is limited with respect to the parameters R_1 and R_2 .

But, the workspace of leg 2 has the advantage along x -axis. That means the workspace can be infinite if the input s is not limited. Practically, this case cannot occur. However, to enlarge the workspace of the robot, we are sure to find a solution that the workspace of leg 1 can be embodied by that of leg 2. Actually, enlarging the workspace is our pursuing objective. In this sense, the workspace of the robot should be that of the leg 1. The workspace of the leg 1 is then our research objective.

For example, the theoretical workspace of leg 1 of the robot with parameters $R_1 = 1.2\text{mm}$, $R_2 = 0.8\text{mm}$ and $R_3 = 0.5\text{mm}$ is shown as the shaded region in Fig. 10. The theoretical workspace and any other type of workspace of the robot can be that which embodies the corresponding workspace of the leg 1 by assigning appropriate values to the parameters L_n ($n=1,2,3$), which will be described in details in the section 7.2. Therefore, in this chapter, the workspace of the leg 1 is regarded as the workspace of the parallel robot. The theoretical workspace is actually bounded by the stationary singularity loci C_{fir_i} and C_{fir_o} . Its area can be calculated by

$$S_{tw} = \pi[(R_1 + R_2)^2 - (R_1 - R_2)^2] = 4\pi R_1 R_2 \quad (21)$$

From Fig. 9, we can see that within the theoretical workspace there is stationary singularity.

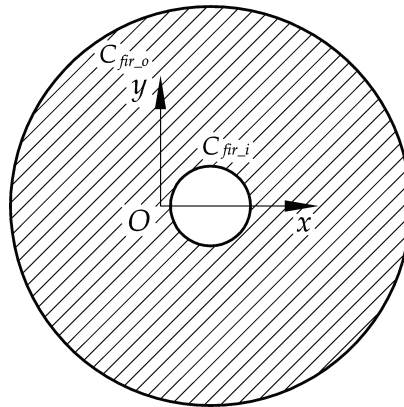


Figure 10. Theoretical workspace of the robot

5.2 Usable workspace

As there exist singular loci inside the theoretical workspace, if a robot wants to move from one point to another it maybe should passes a singular configuration. That means it maybe changes from one working mode to another. In practice, changing working mode during the working process is definitely impossible. Therefore, we should find out a working space without singularity.

The *usable workspace* is defined as the maximum continuous workspace that contains no singular loci inside but bounded by singular loci outside. According to this definition, not every point within the usable workspace can be available for a practical robot. The robot will be out of control at the points on the boundaries and their neighborhoods. But within this region, the robot with a specified working mode can move freely.

In Section 4.2, two kinds of singular loci have been presented for the robot as shown in Fig. 9. The stationary singularity is actually the boundary of a theoretical workspace. Then, a robot with every working mode can have such singular loci. However, as the uncertainty singularity occurs inside the workspace, not every working mode has all such singularities. Normally, for most parallel robots studied here, there are four tangent points between the two kinds of singular loci. The points can be used to identify which singular loci a specified working mode can have. For example, all singular loci of the robot $R_1 = 1.2\text{mm}$, $R_2 = 0.8\text{mm}$ and $R_3 = 0.5\text{mm}$ are shown in Fig. 9. Fig. 11 shows some singular configurations and singular loci of the robot. As shown in Fig. 11, there are four tangent points m , v , q and k between the four singular loci C_{fir_i} , C_{fir_o} , C_{sec_l} and C_{sec_r} . At these four points, both of the stationary and uncertainty singularities occur. The four points divide the singular curves C_{sec_l} and C_{sec_r} into four parts. At the arcs $m1q$ and $v3k$, the robot is in singular only when it is with the “+” mode. At the arcs $m2q$ and $v4k$, the working mode “-” is in singular.

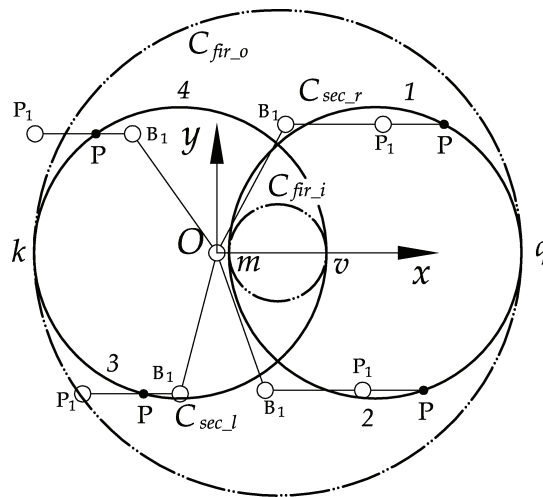


Figure 11. The uncertainty singular loci of a robot with different working modes. What we are concerned about here is the robot with the “+” working mode. Fig. 12 shows all singular loci of such kinds of robots.

The theoretical workspace is divided into two parts by the singular loci shown in Fig. 12, which can be used to identify the usable workspaces of the robots with the “+” working mode and, at the same time, the *down-configuration*. In order to reduce the occupying space, the lower region shown in Fig. 12 is referred to as the *usable workspace* of the parallel robot. They are shown as the shaded region in Fig. 13. Actually, the *usable workspace* is the half of the theoretical workspace. The area can be calculated by

$$S_{uw} = \frac{\pi}{2} [(R_1 + R_2)^2 - (R_1 - R_2)^2] = 2\pi R_1 R_2 \tag{22}$$

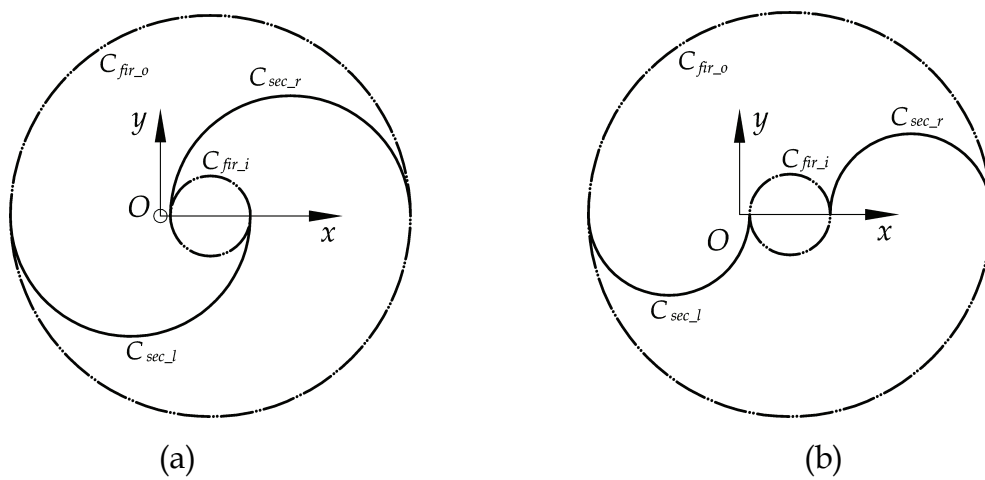


Figure 12. Singular loci of the robot with the “+” working mode: (a) $R_1 \geq R_2$; (b) $R_1 < R_2$

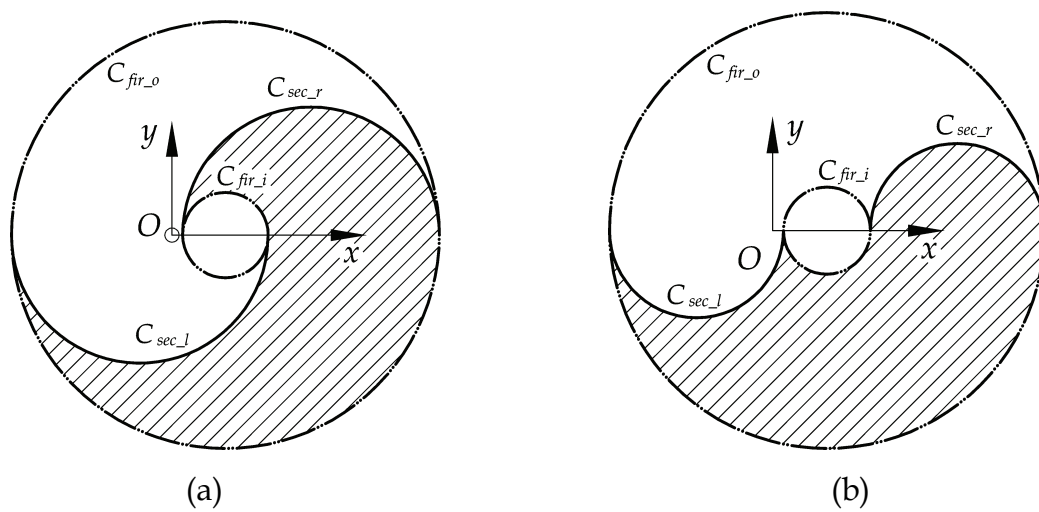


Figure 13. Usable workspace of the robot with both the “+” working mode and *down-configuration*: (a) $R_1 \geq R_2$; (b) $R_1 < R_2$

5.3 Workspace atlas

To apply a specified robot in practice, we usually should determine the link lengths with respect to a desired application. This is actually the so-called optimal kinematic design (parameter synthesis) of the robot. In such a process, one of the most classical tools that has been using is the chart.

Chart is a kind of tool to show the relationship between concerned parameters. As it is well known, the performance of a parallel robot depends not only on the pose of the end-effector but also on the link lengths (dimensions). Disregarding the pose, each of the links can be the length between zero and infinite. And there are always several links in a parallel robot. Then the combination of the links with different lengths will be infinite. They undoubtedly have different performance characteristics. In order to summarize the characteristics of a performance, we must show the relationship between it and geometrical parameters of the parallel robot. To this end, a finite space that must contain all kinds of robots (with different link lengths) should be first developed. Next is to plot the chart considering a desired performance. In this paper, the space is referred to as the design space. The chart that can show the relationship between performances and link lengths is referred to as atlas.

5.3.1 Development of a design space

The Jacobian matrix is the matrix that maps the relationship between the velocity of the end-effector and the vector of actuated joint rates. This matrix is the most important parameter in the field. Almost all performances are depended on this parameter. Therefore, based on the Jacobian matrix, we can identify which geometrical parameter should be involved in the analysis and kinematic design.

For the parallel robot considered here, there are three parameters in the Jacobian matrix (see Eq. (17)), which are R_1 , R_2 and R_3 . Theoretically, any one of the parameters R_1 , R_2 and R_3 can have any value between zero and infinite. This is the biggest difficulty to develop a design space that can embody all robots (with different link lengths) within a finite space. For this reason, we must eliminate the physical link size of the robots.

Let

$$D = (R_1 + R_2 + R_3)/3 \quad (23)$$

One can obtain 3 non-dimensional parameters r_i by means of

$$r_1 = R_1/D, r_2 = R_2/D, r_3 = R_3/D \quad (24)$$

This would then yield

$$r_1 + r_2 + r_3 = 3 \quad (25)$$

From Eq.(25), the three non-dimensional parameters r_1 , r_2 and r_3 have limits, i.e.,

$$0 < r_1, r_2, r_3 < 3 \quad (26)$$

Based on Eqs. (25) and (26), one can establish a design space as shown in Fig. 14(a), in which the triangle ABC is actually the design space of the parallel robot. In Fig. 14(a), the triangle ABC is restricted by r_1 , r_2 and r_3 . Therefore it can be figured in another form as shown in Fig. 14(b), which is referred to as the planar-closed configuration of the design space. In this design space, each point corresponds a kind of robot with specified value of r_1 , r_2 and r_3 .

For convenience, two orthogonal coordinates r and t are utilized to express r_1 , r_2 and r_3 . Thus, by using

$$\begin{cases} r = 2r_1/\sqrt{3} + r_3/\sqrt{3} \\ t = r_3 \end{cases} \quad (27)$$

coordinates r_1 , r_2 and r_3 can be transformed into r and t . Eq. (27) is useful for constructing a performance atlas.

From the analysis of singularity and workspace, we can see that the singular loci and workspace shape of a robot when $r_1 > r_2$ are different from those of the robot when $r_1 < r_2$. For the convenience of analysis, the line $r_1 = r_2$ is used to divide the design space into two regions as shown in Fig. 14(b).

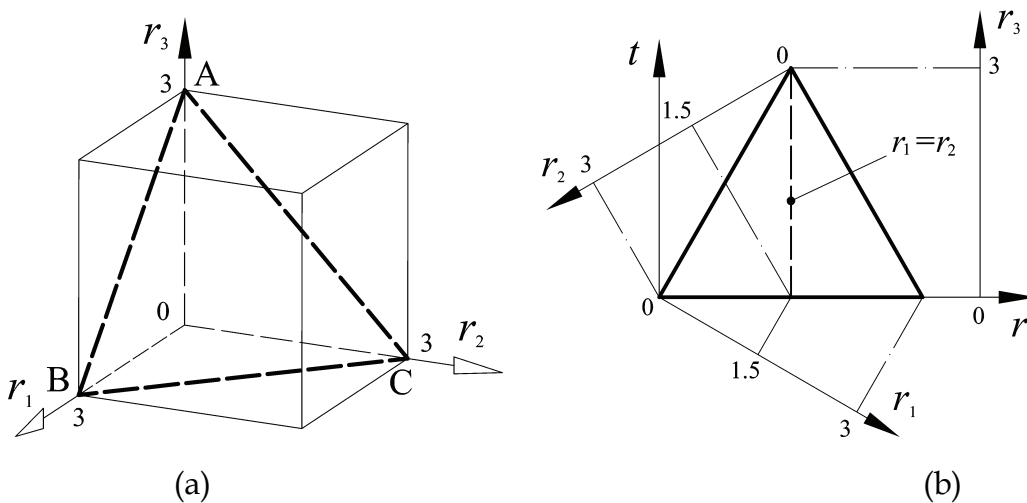


Figure 14. Design space of the 2-DOF translational parallel robot

Thank You for previewing this eBook

You can read the full version of this eBook in different formats:

- HTML (Free /Available to everyone)
- PDF / TXT (Available to V.I.P. members. Free Standard members can access up to 5 PDF/TXT eBooks per month each month)
- Epub & Mobipocket (Exclusive to V.I.P. members)

To download this full book, simply select the format you desire below

